Dual-peak long period fibre grating coated with graphene oxide for label-free and specific assays of H5N1 virus

Binbin Luo[1] | Zhijiang Liu [1] | Xin Wang [1] | Shenghui Shi[1] | Nianbing Zhong [1] | Peijie Ma[2] | Shengxi Wu[2], *| Decao Wu | Mingfu Zhao[1], ** |Wangwang Liang[3]

1 Chongqing Key Laboratory of Optical Fiber Sensor and Photoelectric Detection, Chongqing University of Technology, Chongqing, China

2 School of Pharmacy and Bioengineering, Chongqing University of Technology, Chongqing, China

3 Chongqing Animal Disease Prevention and Control Center, China

*** Correspondence**
Shengxi Wu, Chongqing University of Technology, No. 69 Hongguang Road Banan District, 400054 Chongqing, Country
Email: sxwu2004@cqut.edu.cn;

****Correspondence**
Mingfu Zhao, Chongqing University of Technology, No. 69 Hongguang Road Banan District, 400054 Chongqing, Country
Email: zmf@cqut.edu.cn

Avian influenza is an acute infectious disease caused by the avian influenza virus (AIV), which has caused enormous economic losses and posed considerable threats to public health. This study aimed to demonstrate an immunosensor based on dispersion turning point long-period fiber grating (DTP-LPFG) integrated with graphene oxide (GO) for the specific detection of a type of AIV H5N1 virus. LPFG was designed to work at DTP, whose dual-peak spacing was very high sensitive to a refractive index. Anti-H5N1 monoclonal antibodies were covalently bonded with the GO film on the fiber surface, thus constructing an immunosensor for the label-free and specific detection of the H5N1 virus. The proposed method was capable of the reliable detection of H5N1 virus with the limit of detection as low as ~1.05 ng/mL within the large range of 1–25 μg/mL. More importantly, immunoassays of the whole H5N1 virus in clinical samples further confirmed that the GO-integrated DTP-LPFG immunosensor showed very high specificity to the H5N1 virus and demonstrated great potential for clinical use.

KEYWORDS
biosensor, long period fiber grating, dispersion turning point, graphene oxide, avian influenza virus

1 | INTRODUCTION

Avian influenza, an acute infectious disease caused by avian influenza virus (AIV), has become a new threat to global public health due to its high morbidity and potential mortality. At present, the detection methods of AIV mainly include virus isolation and serum identification (VI-SI) [1], hemagglutination inhibition (HA-HI) tests [2], serum neutralization and enzyme-linked immunosorbent assay (ELISA) [3], molecular diagnostic techniques such as reverse transcription–polymerase chain reaction (RT-PCR) [4], gene chip [5], new-generation high-throughput sequencing method [6], and so forth. However, VI-SI requires complex procedures that take time (from days to weeks) and are cumbersome. The (HA-HI) tests can improve the sensitivity and specificity of detection. However, their sensitivity and specificity depend on the control of AIV RNA, and they have the disadvantages of cross-contamination, cumbersome operation, and high cost.

ELISA is suitable for large-scale serological studies, but it also has disadvantages including high time consumption, complex process, and inconvenient on-site operation. RT-PCR method has high sensitivity because it directly identifies viral genes; however, the high cost of the equipment still restricts the use of this method in clinical practice. Although the new high-throughput sequencing method has high precision and low error rate, its detection requires complex instruments and equipment. Therefore, developing a rapid, accurate, and reproducible detection method to quickly and accurately diagnose and timely detect the possible outbreak of AIV has become a serious challenge for scientific researchers.

In the last several decades, various types of optical fiber (OF) biosensors have been developed in the biological fields for the label-free and real-time detection of bacteria [7], cells [8], proteins [9], peptides [10], immunoglobulin antigens and antibodies [11-13], DNA [14], and so forth, due to their common advantages of smart structure and remote sensing. Of these, the optical fiber grating (OFG)-based biosensors are wavelength encoded, and hence the readout is independent of the optical intensity fluctuation induced by fiber bending or optical source. Cladding etching [15] and side-polished [16] techniques have been used to improve the sensing performance of OFG biosensors, but these methods can destroy the integrity of the fiber structure. Therefore, increasing efforts have been made to design either OFG structures or a thin film coating on OFGs to improve their sensitivity to surrounding refractive index (SRI). The dispersion turning point long-period fiber gratings (DTP-LPFGs) own intrinsic high sensitivity to the SRI [17]. The deposition of a thin film on LPFG induces potential changes in transmission properties. Selecting a thin film with adequate thickness and refractive index can provide the highest sensitivity for SRI.

On the contrary, unique physical and chemical properties of nanomaterials, including carbon nanotube [18-20], graphene [21, 22], two-dimensional black phosphorus [23-25] and transition metal sulfides [26], have gained enormous attention and have been combined with OF or OFGs to realize chemical and biological sensing devices with improved sensitivity and selectivity. Especially graphene oxide (GO), as a derivative of graphene, apart from being a type of lattice-like nanostructure, it displays advantageous of ability for solution processing, very high ratio surface area and excellent capabilities for direct wiring with biomolecules through π-π stack or covalent linking to biomolecules, due to an abundance of carboxyl groups exposed on the edges and hydroxyl groups on its basal plane [27]. Therefore, many GO-integrated OF sensors have been explored for the label-free and ultrasensitive detection in chemical and biological fields [28-31].

In this study, a GO-integrated DTP-LPFG sensor was designed and fabricated using the high sensitivity of DTP-LPFG and the special properties of GO. GO was coated on the surface of DTP-LPFG through hydrogen bonding. Also, anti-H5N1 monoclonal antibodies (anti-H5N1 MAbs) were covalently bonded with the GO film through an amide linkage, thus forming an immunosensor for the label-free and highly specific detection of the H5N1 virus, which is a common type of AIV. Sensing performances of GO-integrated DTP-LPFG immunosensors were evaluated by detecting highly purified H5N1 virus in buffer solutions. The immunosensor was used in clinical immunoassays for AIV-Blank allantoic fluid, Newcastle disease virus (NDV) allantoic fluid, and AIV allantoic fluid to evaluate the specific and clinical performances of the immunosensor to the whole H5N1 virus. This study was novel in using a GO-integrated OFG immunosensor for the label-free and specific detection of H5N1 virus and effective diagnosis of the whole H5N1 virus in a clinical allantoic fluid.

2 | Material and Method

2.1 | Preparation of Reagents

All the reagents were of analytical grade, and each working solution was prepared with sterilized deionized water. GO suspension (2 mg/mL) was purchased from Xianfeng Company (Nanjing, China). Hydrofluoric acid (HF) solutions (40%), sodium hydroxide (NaOH, 99% purity), dilute nitric acid solutions (HNO_3, 5%), anhydrous ethanol (C_2H_6O), *n*-hydroxysuccinimide (NHS, 99% purity), and 1-(3-dimethylaminopropyl)-3-ethylcarbodiimine (EDC, 99% purity) were purchased from Sigma–Aldrich, China. Phosphate-buffered saline (PBS, pH 7.4) was obtained from Wuhan Boster Biological Technology Co., China. A 4-morpholineethane-sulfonic acid hydrate (MES, 0.1 m, pH = 6.0) buffer was purchased from Shanghai General Chemical Reagent Factory, China. Anti-H5N1 MAbs (70 kDa, purity >90%, 2 mg/mL) was purchased from Abcam Co., USA.

Trimethylmethylaminomethane (Tris) and Tween were purchased from GEN-View Inc., USA. The home-made skimmed milk powder sealing fluid (SMPSF) is a mixture of skimmed milk powder, Tween, and Tris-buffered saline (TBS, 0.1M, pH = 7.4) in a certain ratio, which was used in this study for sealing the free carboxyl terminals of the GO film on the fiber surface.

The H5 AIV strain was a kind gift from the Veterinary Department, Nanjing Agricultural University. The attenuated H5N1 subtype AIV strain was kindly provided by Chongqing Animal Disease Prevention and Control Center, China. The NDV-AV29 strain was purchased from the China Institute of Veterinary Drug Control. SPF chick embryos (aged 9 days) were inoculated with diluted H5-AIV (0.2 mL) into the allantoic cavity to prepare the AIV allantoic fluid. The eggs

were hatched at 37°C for 72 h, followed by allantoic fluid collection. The NDV allantoic fluid was prepared in the same way as the AIV allantoic fluid.

2.2 | Working principle of DTP-LPFG

The phase-matching condition of LPFG was expressed as [32]:

$$\boldsymbol{\lambda_{res}} = \left(\boldsymbol{n_{eff}^{co}} - \boldsymbol{n_{eff}^{cl,m}}\right)\boldsymbol{\Lambda} \quad (1)$$

where $\boldsymbol{\lambda_{res}}$ is the resonance wavelength, $\boldsymbol{n_{eff}^{co}}$ and $\boldsymbol{n_{eff}^{cl,m}}$ are the effective refractive index (RI) of the core mode and m-order cladding mode, respectively, and $\boldsymbol{\Lambda}$ is the grating period. When the SRI changed, the resonance wavelength shift of LPFG was given by [33]:

$$\frac{d\lambda_{res}^{m}}{d_{sur}} = -\boldsymbol{\lambda_{res}^{m}} \cdot \frac{d\lambda_{res}^{m}/d\Lambda}{n_{eff}^{co}-n_{eff}^{cl,m}} \cdot \frac{u_m^2 \lambda_{res}^{m} n_{sur}}{8\pi r_{cl}^3 n_{cl}\left(n_{eff}^{co}-n_{eff}^{cl,m}\right)\left(n_{cl}^2-n_{sur}^2\right)^{3/2}} \quad (2)$$

where, $\boldsymbol{\lambda_{res}^{m}}$ is the resonance wavelength of m-order coupled mode; $\boldsymbol{u_m}$ is the root of the first class of zero-order Bessel functions; $\boldsymbol{n_{sur}}$ is the RI of the surrounding medium; $\boldsymbol{r_{co}}$ and $\boldsymbol{r_{cl}}$ are LPFG core and cladding radius, respectively. The results of a previous study [17] showed a turning point in the phase matching curve for the standard single-mode fiber, when $\boldsymbol{\Lambda}$ is small enough ($80\boldsymbol{\mu m} < \boldsymbol{\Lambda} < \boldsymbol{300\mu m}$) . Two discontinuous resonant wavelengths were coupled to the same cladding mode on both sides of the turning point, resulting in a double-resonance peak. For the purpose of guaranteeing the dual peaks to locate at the NIR band that the commercial optical equipment usually used (i.e., 1250 -1650nm), the grating period of LPFG should be designed to be between 130-150 μm by using the simulated results of the couple-mode theory [17]. According to Eq. (2), for the resonance wavelength at the positive dispersion point (the shorter wavelength peak, $\boldsymbol{d\lambda_{res}^{m}/d\Lambda > 0}$), it would blue shift with the increase in SRI; while for the resonance wavelength at the negative dispersion point (the longer wavelength peak, $\boldsymbol{d\lambda_{res}^{m}/d\Lambda < 0}$), it would red shift. Hence, the variation for the separation of the dual peaks could change with the response of DTP-LPFG to the surrounding, such as the SRI change, biochemical reaction or combination of biomolecules. Furthermore, it was proved that the deposition of the GO film on the surface of LPFGs could further improve its SRI sensitivities [34].

2.3 | Fabrication of DTP-LPFG immunosensor

2.3.1 | Fabrication and properties of GO-integrated DTP-LPFG

Quasi-continuous KrF laser (wavelength 248 nm) and scan mask technology were used to write LPFG on the H_2-loaded single-mode fiber (SMF-28). After the preparation of DTP-LPFG, it was annealed in a convection oven at 80℃ for 24 h to ensure the stability of spectral characteristics. The obtained DTP-LPFG had a grating period of 136 μm and a length of 19 mm, resulting in dual peaks at ~1375 nm and ~1540 nm (exposed in the air), as shown in Figure 1(a), which was in accordance with the theoretical expectation and designation. The calibration for the SRI sensitivity of the dual-peak separation was ~795 nm/RIU, with the left peak and right peak being ~–306 nm/RIU and ~489 nm/RIU for the low RI range of 1.333–1.38, respectively, which were ~40 times higher than those (~20 nm/RIU) for the normal LPFGs.

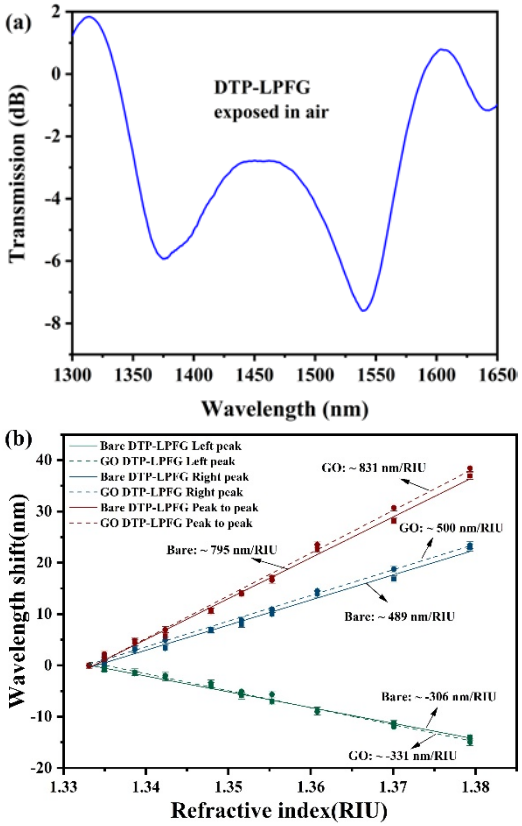

FIGURE 1 (a) A spectrum of DTP-LPFG exposed in the air; (b) calibrations of the SRI sensitivity of the DTP-LPFG sensor before and after GO coating.

The process of GO coating on fiber surface followed several steps. First, DTP-LPFG was immersed in HNO_3 (5% *v*/*v*) solution for 2 h and then rinsed thoroughly with ultrapure water and ethanol. Subsequently, DTP-LPFG was immersed in NaOH (0.2M) solution for 3.5 h in a thermostat at 40°C and then for another 0.5 h at room temperature so as to activate the –OH group on the fiber surface. The grating surface was repeatedly rinsed with ultrapure water to remove excess impurities and then dried in a convection oven at 50°C for 10

min. Finally, the DTP-LPFG sensor was incubated in GO suspension (2 mg/mL) at room temperature for 12 h; GO was combined with the fiber surface through a hydrogen bond. The fiber surface was repeatedly rinsed with ultrapure water and ethanol to flush away the unbound GO, and hence GO-integrated DTP-LPFG was obtained.

The surface morphology of GO-integrated DTP-LPFG was investigated using a field emission scanning electron microscope (FESEM, ZEISS Sigma HD^{TM}). As shown in Figure 2(a–d), a dense membrane layer with wrinkles covered the fiber surface after the GO coating. It can be seen from Fig. 2(a) that the GO coating on fiber surface is not so homogeneous, with the darker areas being relatively thicker GO layers and the brighter areas being the relatively thinner ones. This should be due to that the used GO suspension was consist of multi-layer GO (1 - 6 layers, average thickness 0.8-5 nm, lateral size 0.5 - 5 μm). In addition, the elements of the fiber surface analyzed by using the FESME accessory—energy dispersive spectrometer (EDS), the maximum detection depth of which is ~1000 nm. As shown in Fig. 2(e), it is clear that the fiber surface containing C, O and Si elements, which is in accordance with components of GO and SiO_2. Hence, the aforementioned results provided good evidence for the GO coating on the fiber surface.

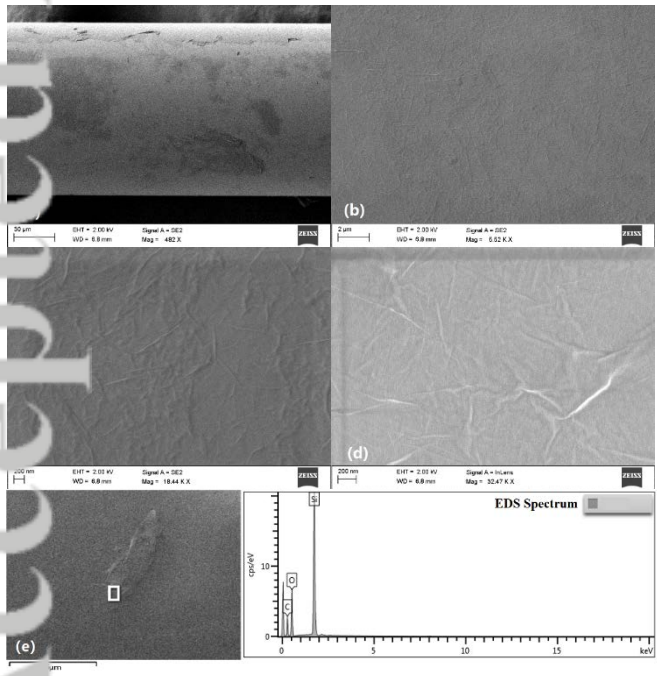

FIGURE 2 FESEM images of GO-integrated DTP-LPFG: (a) 482 X; (b) 5.52 KX; (c) 18.44 KX; (d) 32.47 KX; and (e) the corresponding EDS spectrum. Note: (a), (b), (c) is the side-edge detection mode, while (d) is the center detection mode; and the EDS spectrum graph on the left of (e) is corresponding to the highlighted dot on the right.

The calibration of the SRI sensitivity is also shown in Figure 1(b), indicating that the SRI sensitivity of the dual-peak separation was ~832 nm/RIU, with the left peak and right peak being ~–331 nm/RIU and ~500 nm/RIU for the low RI range of 1.333–1.38, respectively, which increased by ~5% compared with those for bare DTP-LPFG. Because the GO film on the fibre surface would increase the effective RI of cladding mode ($n_{eff}^{cl,m}$) of the DTP-LPFG sensor, thus according to Eq. (2), the RI sensitivities of the dual peaks would increase correspondingly. However, the enhancement of RI sensitivity is not high due to the GO film on fibre surface was very thin, but the GO layer could provide abundant binding sites for biomolecules, which will, to a great extent, affect the sensitivity and detection range when it was used as a biosensor.

2.3.2 | Bio-functionalization of GO-integrated DTP-LPFG

EDC (0.004 g) and NHS (0.002 g) were dissolved in 200 μL of ultrapure water with a mass ratio of 2:1. Then, MES buffer (300 μL) was mixed to obtain an EDC/NHS-activating system. Then, the GO-integrated DTP-LPFG sensor was immersed in EDC/NHS solution (300 μL) for 1 h at room temperature to activate the −COOH groups on the fiber surface. The GO-integrated DTP-LPFG sensor was then incubated in anti-H5N1 MAbs solution (50 μg/mL, 300 μL) for 1 h at room temperature, during which the grating was placed in different positions of the solution every 20 min to ensure adequate anti-H5N1 MAbs to combine with the GO film through an amide linkage. The sensor was repeatedly washed with blank PBS to remove unbound anti-H5N1 MAbs from its surface. Finally, the GO-integrated DTP-LPFG sensor was immersed in the configured SMPSF for 1 h to seal the remained carboxyl terminal of the GO film. The whole surface modification process for the fiber surface is illustrated in Figure 3.

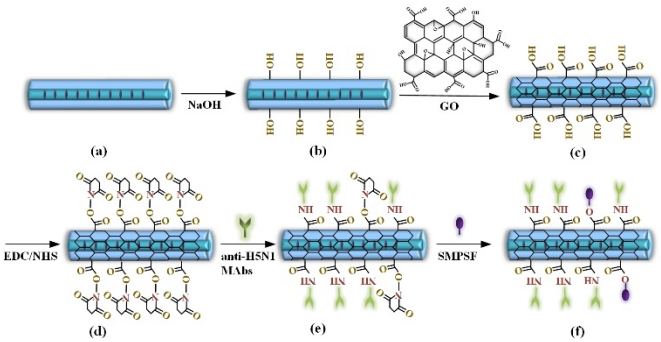

FIGURE 3 Surface modification process for DTP-LPFG: (a) bare fiber; (b) hydroxylation; (c) GO coating; (d) EDC/NHS treatment; (e) immobilization of anti-H5N1 MAbs; (f) sealing by SMPSF.

2.4 | Experimental Scheme

Figure 4 shows the experimental system for monitoring the transmission spectrum of the GO-integrated DTP-LPFG sensor. Broadband light was generated using the supercontinuous laser source (SC-5, 480–2200 nm). The attenuator reduced the power of the light output to 80%, not only ensuring the spectral stability of the light source but also preventing damage to the OE path. The light was delivered to DTP-LPFG through SM28 fiber after passing the isolator, the function of the isolator was to block the backscattering and reflected light. The transmission spectrum of the sensor was recorded with an optical spectrum analyzer (OSA, MS9740A, minimum resolution 0.03 nm). Inset in Figure 4 shows the the fluidic part of the setup, including two parallel settled glass slides with and a mobilizable one between them. The ends of DTP-LPFG were fixed on the two settled glass slides, and thus the grating across upon the top surface of the mobilizable one. In the experiments, the working solution was dropped on the top surface of the mobilizable glass slide to cover the grating area, and was thrown away with the mobilizable glass slide after each test. During the experiment, it was essential to guarantee the free horizontal state of DTP-LPFG and keep the laboratory temperature constant (25℃) to avoid the detection error caused by sensor cross-sensitivity effects induced by the strain and temperature.

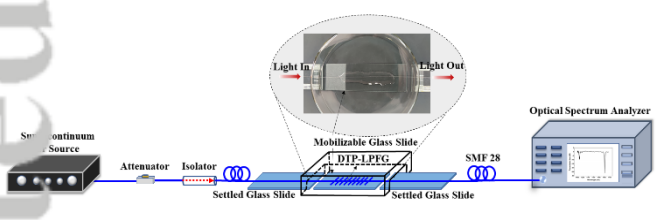

FIGURE 4 An experimental system for monitoring the spectrum of the sensor (Inset: the fluidic part of the experimental setup).

Highly purified H5N1 virus dissolved in PBS were used to evaluate the sensing performances of the GO-integrated DTP-LPFG immunosensor. Using the experimental setup in Figure 1, blank PBS (200 µL) was first introduced into the sensing region and the observed spectrum was recorded as the reference. Subsequently, the prepared H5N1 virus solutions (200 µL) were used for immunoassays from the lowest to the highest concentration, including 1 ng/mL, 5 ng/mL, 10 ng/mL, 20 ng/mL, 20 ng/mL, 50 ng/mL, 100 ng/mL, 200 ng/mL, 500 ng/mL, 1 µg/mL, 5 µg/mL, 10 µg/mL, 25 µg/mL, 50 µg/mL, and 100 µg/mL. The spectrum of the immunosensor was monitored online by an OSA and recorded every 3 min until it became stable at each testing concentration level. After completing each assay for H5N1 virus solution, the immunosensor was washed with blank PBS to remove the unbonded H5N1 virus on the fiber surface and immersed in blank PBS again. Finally, the dual-peak spacing of the immunosensor was recorded as the corresponding readout of the immunoreaction.

The specificity and clinicality are important criteria to evaluate the eligibility of the immunosensor. After completing the aforementioned assays for highly purified H5N1 virus solutions, the GO-integrated DTP-LPFG immunosensor was etched using HF solution (5% *v*/*v* in deionized water) for 5 min. As a consequence, all the layers on the fiber surface were removed without affecting the geometrical structure and sensing properties of DTP-LPFG during the etching process. The bare DTP-LPFG was disposed by the same surface modification processes, as mentioned earlier. The evaluating scheme had three steps, including immunoassays for AIV-Blank allantoic fluid, NDV allantoic fluid, and AIV allantoic fluid. It is worth to point out here that, in the experiment the H5N1 antigen diluted by PBS is the purified H5N1 virus. The total length of H5N1 virus genome is about 13.6kb. The composition of H5N1 virus in PBS solution is single, but the composition of clinical samples is complex. The allantoic fluids contained many biomolecular impurities (e.g., heteroproteins, biosalts, cells, etc.). Apart from these, the AIV allantoic fluid contained the H5N1 virus, which was not present in the AIV-Blank allantoic fluid and NDV allantoic fluid. Therefore, these three immunoassay steps could identify the specificity of the AIV immunosensor for binding to the H5N1 virus, proving its potential clinical applications.

3 | RESULTS AND DISCUSSION

3.1 | Surface modification monitored by the spectrum of DTP-LPFG

In the experiment, spectral monitoring was also conducted for each surface modification of DTP-LPFG, and the spectral test for each step was conducted in blank PBS. Fig. 5 (a) and (b) show the spectral evolution and the corresponding changes for the wavelength separation of the dual-peaks during the whole modification process. It can be seen that the shorter- and longer-wavelength one of the dual-peaks would blue shift and red shift, respectively, as the additional layers deposited on fiber surface gradually. This is because the effective RI of cladding modes would increase as an additional layer deposited on fiber surface, thus according to the analyses by Eq. (2), the dual-peaks would shift in an opposite direction.

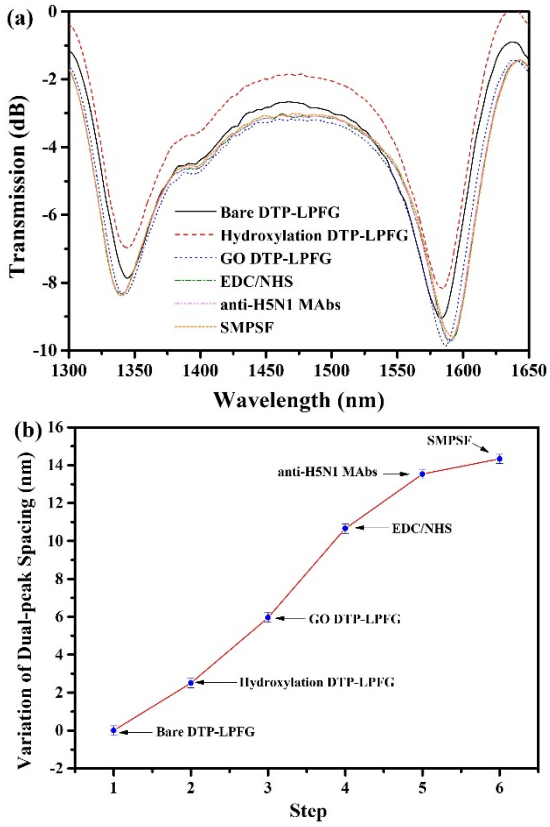

FIGURE 5 (a) Spectral evolution and (b) corresponding variations for the dual-peak spacing of DTP-LPFG during the whole modification process, the error bars were obtained from the wavelength accuracy of the optical spectrum analyzer.

The relative variation of the dual-peak separation of DTP-LPFG was ~2.5025 nm, ~3.465 nm, ~4.69 nm, ~2.8725 nm, and ~0.7975 nm in the steps of hydroxylation, GO deposition, carboxyl activation of GO, immobilization of anti-H5N1 MAbs, and SMPSF sealing for the remaining carboxyl sites, respectively. These changes for the dual-peak spacing also provided proofs for the effective surface modification on the fiber surface.

3.2 | Detection of H5N1 virus in PBS solution

Figure 6(a) is the variation of the dual-peak spacing against testing time during the whole detection process in which the H5N1 virus concentration increased from 1 ng/mL to 100 µg/mL. Figure 6(b) shows the corresponding spectra of the immunosensor. The total change in the dual-peak spacing of the immunosensor was ~10.56 nm, and it gradually became saturated at the point larger than 25 µg/mL due to the fewer specific binding sites for H5N1 antigen. The change in the dual-peak spacing of the immunosensor was ~0.90 nm for the concentration of 1 ng/mL, indicating that it showed a good response in the low-concentration area in the initial use. At the same time, the aforementioned immune tests showed that the spectrum usually took only 10–20 min to reach the stable statue at each measured concentration level. Thus, the proposed immunosensor had the ability of fast detection for H5N1 virus.

Furthermore, Figure 6(c) shows the relationship between the variation of dual-peak spacing and the concentration of H5N1 virus illustrated in Figure 6(a). The specific adsorption of H5N1 antigen by the immunosensor followed the Langmuir model given by [35]:

$$\frac{C}{\Delta\lambda} = \frac{C}{\Delta\lambda_{max}} + \frac{1}{\Delta\lambda_{max}} \cdot K_d \quad (3)$$

where C is the concentration of H5N1 virus solution and $\Delta\lambda$ is the corresponding variation of the dual-peak spacing; $\Delta\lambda_{max}$ is the max variation of dual-peak spacing in the whole immunoassay process; and K_d is the dissociation coefficient describing the binding ability of two interacting molecules (i.e., H5N1 antigens and anti-H5N1 MAbs), which was calculated to be 5.31×10^{-9} M according to the experimental data in Figure 6(c), suggesting good affinity of the immunosensor to H5N1 virus.

The limit of detection (LOD) is one of the most important parameters for biosensors. According to the method proposed by the International Union of Pure and Applied Chemistry, the LOD of the immunosensor was calculated as described in [36]:

$$x_{LOD} = f^{-1}(\overline{y}_{blank} + 3\sigma_{max}) \quad (4)$$

where $\overline{y}_{blank}$ is the readout of the immunosensor measured in blank PBS, and σ_{max} is the corresponding standard deviation; f^{-1} represents the inverse function of the fitting cure obtained in Figure 6(c). In this study, the LOD of the immunosensor was calculated to be ~1.05 ng/mL. This value was ~1619 times better than that detected by the widely used gold diagnostic method (~1.7 µg/mL) [37]. Therefore, considering the aforementioned analysis, the detection range of the proposed immunosensor for H5N1 virus was estimated as 1 ng/mL to 25 µg /mL.

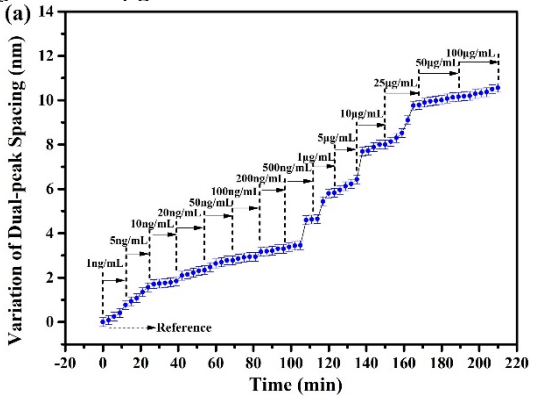

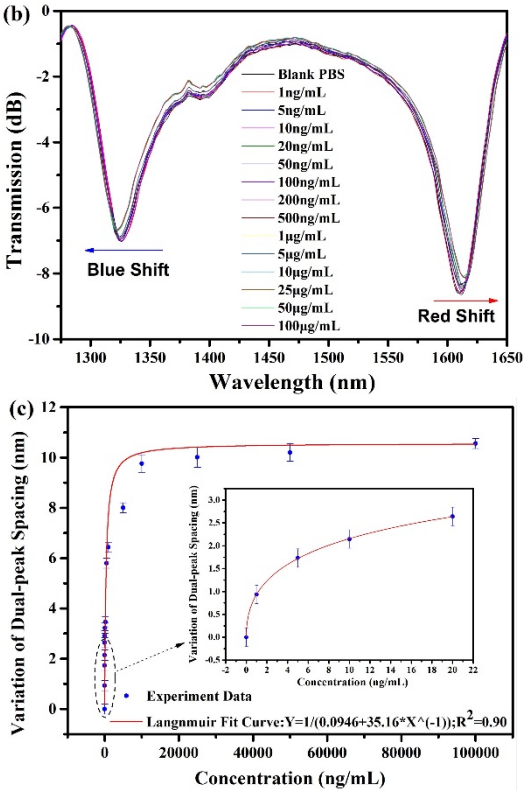

FIGURE 6 (a) Variation of the dual-peak spacing against testing time during the whole detection process, the error bars were obtained from the wavelength accuracy of the optical spectrum analyzer; (b) the corresponding spectral evolution of DTP-LPFG during the whole modification process; and (c) variation of the dual-peak spacing against the concentration of H5N1 virus solutions, inset is the response in the range of 0 – 20 ng/mL, the error bars were obtained from the averaging of five independent measurements.

3.3 | Evaluation for the specificity and clinical performances of the immunosensor

The spectrum of the GO-integrated DTP-LPFG immunosensor immersed in blank PBS was recorded as the reference. Immunoassays were conducted for the prepared AIV-Blank allantoic fluid (300 μL) first and then NDV allantoic fluid (300 μL). The prepared AIV allantoic fluid (300 μL) containing different concentrations of the H5N1 virus, including 1 ng/mL, 5 ng/mL, 100 ng/mL, 10 μg/mL, 25 μg/mL, and 50 μg/mL, were used for immunoassays successively. These AIV allantoic fluids were viral concentrates obtained by H5N1 virus amplification, while the NDV allantoic fluid was obtained by NDV virus amplification. Therefore, the immunoassays in the allantoic fluid had clinical applications.

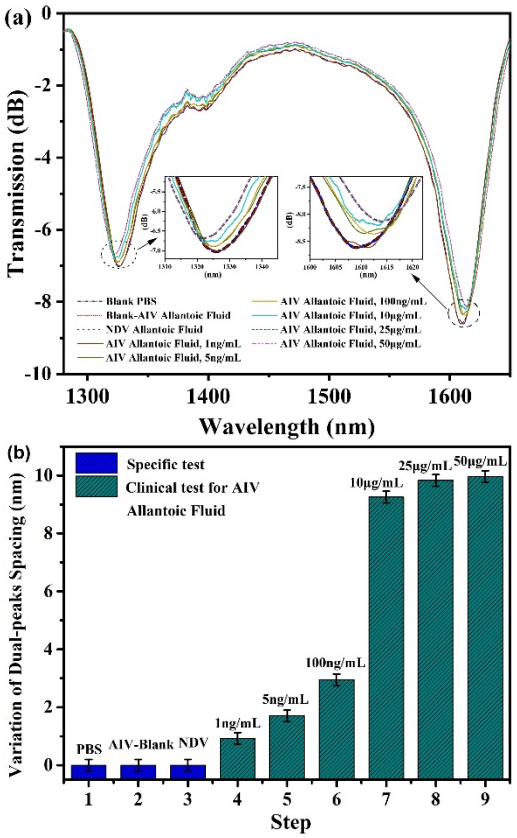

FIGURE 7 (a) Spectral evolution (Inset: the magnification graphs for the dual-peak movements), and (b) the corresponding variations for the dual-peak spacing of the GO-DTP-LPFG immunosensor during the specific and clinical tests, the error bars were obtained from the averaging of five independent measurements.

Similarly, following each test (20 min) for every allantoic fluid, the immunosensor was washed with blank PBS several times and then immersed in blank PBS again. Hence, the spectrum of the immunosensor was recorded. Figure 7(a) and 7(b) shows the spectral evolution of the sensor during the immunoassay and the corresponding dual-peak spacing of the DTP-LPFG immunosensor, respectively. The dual-peak spacing of the immunosensor remained nearly unchanged for the immunoassays of AIV-Blank allantoic fluid and NDV allantoic fluid. Consequently, no H5N1 virus was found in these two clinical samples. Nevertheless, for the immunoassays in the AIV allantoic fluid, the dual-peak spacing of the immunosensor increased with the concentration of the H5N1 virus in the clinical samples. As a consequence, these assays proved that the proposed GO-integrated DTP-LPFG immunosensor had very high specificity to the H5N1 virus and demonstrated great potential in clinical use.

Furthermore, Figure 7(b) shows that the variation of the dual-peak spacing of the immunosensor was ~0.93 nm, ~1.705 nm, ~2.94 nm, ~9.26 nm, ~9.83 nm, and ~9.96 nm for the test

of AIV allantoic fluid with H5N1 virus concentration of 1 ng/mL, 5 ng/mL, 100 ng/mL, 10 μg/mL, 25 μg/mL, and 50 μg/mL, respectively. Figure 6(a) shows that the variation of the dual-peak spacing of the immunosensor was ~0.90 nm, ~1.57 nm, ~3.16 nm, ~8.1 nm, ~9.76 nm, and ~10.13 nm, respectively, for the test of H5N1 virus with the same concentration in PBS. The average relative deviation for these two sets of experimental data was calculated to be only ~7.6%, manifesting that, even in the assays for clinical samples, the proposed immunosensor showed similar performances as good as those in the pure environments. In addition, the results also indicated that the reprocessed GO-integrated DTP-LPFG immunosensor was reusable with good repeatability.

4 | CONCLUSION

The present study proposed an effective H5N1 virus detecting technique based on DTP-LPFG immunosensor, which was successfully biofunctionalized with anti-H5N1 MABs covalently bonded with the GO film on the fiber surface through amide linkages. FESEM images and electronic energy techniques provided convincing evidence for the effective coating of GO on the fiber surface. Online monitoring for the spectrum of DTP-LPFG during the whole modification process also confirmed every effective modified step. The correlation between the concentration of H5N1 virus in PBS and the variation of dual-peak spacing of DTP-LPFG was analyzed in detail. The results indicated that the LOD of the proposed immunosensor for H5N1 virus was as low as ~1.05 ng/mL within the range of 1 ng/mL to 25 μg /mL, which was improved ~16.9 times compared with the LOD using the commonly used gold diagnostic method. The immunoassays using the proposed immunosensor for clinical samples confirmed that the immunosensor was highly specific to the whole H5N1 virus, and its testing performances were similar to those tested in the pure environments, thus confirming its great potential for clinical use.

ACKNOWLEDGMENTS

This paper was supported by National Natural Science Foundation of China (61875026), the Foundation and cutting-edge Research Projects of Chongqing Science and Technology Commission(cstc2019jcyj-msxmX0093), the science and technology project of Chongqing Education Commission (KJQN201801121, KJZD-K201901101), Chongqing Technology Innovation and application development project (cstc2019jscx-msxmX0370) and Graduate Student Innovation Program of Chongqing University of Technology (ycx20192046, ycx20192048).

AUTHOR CONTRIBUTIONS

(Binbin Luo, Shengxi Wu and Mingfu Zhao were involved in conceptualization, investigation and designing experiments. Shenghui Shi and Nianbing Zhong was involved in designation and fabrication of the DTP-LPFG sensor. Zhijiang Liu and Xin Wang were involved in performing the experiments, data processed and writing the paper. Wangwang Liang and Peijie Ma were involved in mading AIV-Blank allantoic fluid, AIV allantoic fluid and NDV-allantoic fluid. Decao Wu participated in the coordination of the study and reviewed the manuscript. All authors read and approved the final manuscript.)

CONFLICT OF INTEREST

The authors declare no financial or commercial conflict of interest.

REFERENCES

[1] A. Sakurai and F. Shibasaki, Updated values for molecular diagnosis for highly pathogenic avian influenza virus, *Viruses* **2012**, *4*, 1235.

[2] R. Shiraishi, A. Nishiguchi, K. Tsukamoto and M. Muramatsu, Comparison of commercial enzyme-linked immunosorbent assay kits with agar gel precipitation and hemagglutination-inhibition tests for detecting antibodies to avian influenza viruses, *J. Vet. Med. Sci.* **2012**,*74*,1217.

[3] Y. S. Sun, J. P. Landry, Y. Y. Fei, X. D. Zhu, J. T. Luo, X. B. Wang and K. S. Lam, Effect of fluorescently labeling protein probes on kinetics of protein− ligand reactions, *Langmuir* **2008**, *24*, 13399.

[4] D. J. Alexander, Avian influenza–diagnosis, *Zoonoses public health* **2008**, *55*, 16.

[5] X. Li, X. Qi, L. Miao, Y. Wang, F. Liu, H. Gu, S. Lu, Y. Yang and F. Liu, Detection and subtyping of influenza A virus based on a short oligonucleotide microarray, *Diagn. Microbiol. Infect. Dis.* **2009**, *65*, 261.

[6] J. Shendure and H. Ji, Next-generation DNA sequencing, *Nat. Biotechnol.* **2008**, *26*, 1135.

[7] S. Rajesh, U. Sharath, M. Swetha, A. Sundarrajan and S. G. Sai, Bare fiber Bragg grating immunosensor for real-time detection of Escherichia coli bacteria, *J. Biophotonics* **2017**, *10*, 224.

[8] C. Caucheteur, V. Malachovsk, C. Ribaut and R. Wattiez, Cell sensing with near-infrared plasmonic optical fiber sensors, *Opt. Laser Technol.* **2016**, *78*, 116.

[9] P. Pilla, A. Sandomenico, V. Malachovská, A. Borriello, M. Giordano, A. Cutolo, M. Ruvo and A. Cusano, A protein-based biointerfacing route toward label-free immunoassays with long period gratings in transition mode, *Biosens. Bioelectron.* **2012**, *31*, 486.

[10] S. Sridevi, K. S. Vasu, S. Asokan and A. K. Sood, Sensitive detection of C-reactive protein using optical fiber Bragg gratings, *Biosens. Bioelectron.* **2015**, *65*, 251.

[11] M. P. DeLisa, Z. Zhang, M. Shiloach, S. Pilevar, C. C. Davis, J. S. Sirkis and W. E. Bentley, Evanescent wave long-period fiber Bragg grating as an immobilized antibody biosensor, *Anal. Chem.* **2000**, *72*, 2895.

[12] F. Chiavaioli, P. Biswas, C. Trono, S. Jana, S. Bandyopadhyay, N. Basumallick, A. Giannetti, S. Tombelli, S. Bera, A. Mallick and F. Baldini, Sol–gel-based titania–silica thin film overlay for long period fiber grating-based biosensors, *Anal. Chem.* **2015**, *87*, 12024.

[13] F. Chiavaioli, P. Biswas, C. Trono, S. Bandyopadhyay, A. Giannetti, S. Tombelli, N. Basumallick, K. Dasgupta and F. Baldini, Towards sensitive label-free immunosensing by means of turn-around point long period fiber gratings, *Biosens. Bioelectron.* **2014**, *60*, 305.

[14] D. Sun, T. Guo, Y. Ran, Y. Huang and B. Guan, In-situ DNA hybridization detection with a reflective microfiber grating biosensor, *Biosens. Bioelectron*, **2014**, *61*, 541.

[15] X. Chen, K. Zhou, L. Zhang and L. Bennion, Simultaneous measurement of temperature and external refractive index by use of a hybrid grating in D fiber with enhanced sensitivity by HF etching, *Appl. Opt.* **2005**, *44*, 178.

[16] H. S. Jang, K. N. Park, J. P. Kim, S. J. Sim, O. J. Kon, Y. G. Han and K. S. Lee, Sensitive DNA biosensor based on a long-period grating formed on the side-polished fiber surface, *Opt. Express* **2009**, 17, 3855.

[17] X. Shu, L. Zhang and I. Bennion, Sensitivity characteristics near the dispersion turning points of long-period fiber gratings in B/Ge codoped fiber, *Opt. Lett.* 2001, *26*, 1755.

[18] V. A. Margulis and E. A. Gaiduk, Nature of near-infrared absorption in single-wall carbon nanotubes, *Phys. Lett. A* **2001**, *281*, 52.

[19] S. Y. Set, H. Yaguchi, Y. Tanaka and M. Jablonski, Laser mode locking using a saturable absorber incorporating carbon nanotubes, *J. Lightwave Technol.* **2004**, *22*, 51.

[20] K. K. Chow, S. Yamashita and S. Y. Set, Four-wave-mixing-based wavelength conversion using a single-walled carbon-nanotube-deposited planar lightwave circuit waveguide, *Opt. Lett.* **2010**, *35*, 2070.

[21] . Novoselov, A. K. Geim, S. V. Morozov, D. Jiang, Y. Zhang, S. V. Dubonos, I. V. Grigorieva and A. A. Firsov, Electric field effect in atomically thin carbon films, *Science* **2004**, *306*, 666.

[22] Y. Shao, J. Jang, H. Wu, J. Liu, I. A. Aksay and Y. Lin, Graphene based electrochemical sensors and biosensors: a review, *Electroanalysis* **2010**, *22*, 1027.

[23] E. S. Reich, Phosphorene excites materials scientists, *Nature* **2014**, *506*, 19.

[24] L. Li, Y. Yu, G. J. Ye, Q. Ge, X. Ou, H. Wu, D. Feng, X. H. Chen and Y. Zhang, Black phosphorus field-effect transistors, *Nat. Nanotechnol.* **2014**, *9*, 372.

[25] H. Liu, A. T. Neal, Z. Zhu, Z. Luo, X. Xu, D. Tománek and P. D. Ye, Phosphorene: an unexplored 2D semiconductor with a high hole mobility, *ACS nano* **2014**, *8*, 4033.

[26] Y. Luo, C. Chen, K. Xia, S. Peng, H. Guan, J. Tang, H. Lu, J. Yu, J. Zhang, Y. Xiao and Z. Chen, Tungsten disulfide (WS_2) based all-fiber-optic humidity sensor, *Opt. Express* **2016**, *24*, 8956.

[27] D. P. Singh, C. E. Herrera, B. Singh, S. Singh, R. K. Singh and R. Kumar, Graphene oxide: An efficient material and recent approach for biotechnological and biomedical applications, *Mater. Sci. Eng. C* **2018**, *86*, 173.

[28] J. Lee, J. Kim, S. Kim and D.Min, Biosensors based on graphene oxide and its biomedical application, *Adv. Drug Delivery Rev.* **2016**, *105*, 275.

[29] Y. Huang, B. Yu, T. Guo and B. Guan, Ultrasensitive and in situ DNA detection in various pH environments based on a microfiber with a graphene oxide linking layer, *RSC Adv.* **2017**, *7*, 13177.

[30] Y. Wang, C. Shen, W. Lou, F. Shentu, C. Zhong, X. Dong and L. Tong, Fiber optic relative humidity sensor based on the tilted fiber Bragg grating coated with graphene oxide, *Appl. Phys. Lett.* **2016**, *109*, 031107.

[31] B. Jiang, K. Zhou, C. Wang, Q. Sun, G. Yin, Z. Tai, K. Wilson, J. Liu, X. Zhao, and L. Zhang, Label-free glucose biosensor based on enzymatic graphene oxide-functionalized tilted fiber grating, *Sensors and Actuator B: Chemical* **2017**, *254*, 1033.

[32] A. M. Vengsarkar, P. J. Lemaire, J. B. Judkins, V. Bhatia, T. Erdogan and J. E. Sipe, Long-period fiber gratings as band-rejection filters, *J. Lightwave Technol.* **1996**, *14*, 58.

[33] X. Shu, L. Zhang and I. Bennion, Sensitivity characteristics of long-period fiber gratings, *J. Lightwave Technol.* **2002**, *20*, 255.

[34] C. Liu, Q. Cai, B. Xu, W. Zhu, L. Zhang, J. Zhao and X. Chen, Graphene oxide functionalized long period grating for ultrasensitive label-free immunosensing, *Biosens. Bioelectron.* **2017**, *94*, 200.

[35] B. R. Li, C. W. Chen, W. L. Yang, T. Y. Lin, C. Y. Pan and Y. T. Chen, Biomolecular recognition with a sensitivity-enhanced nanowire transistor biosensor, *Biosens. Bioelectron.* **2013**, *45*, 252.

[36] F. Chiavaioli, C. A. J. Gouveia, P. A. S. Jorge and F. Baldini, Towards a uniform metrological assessment of grating-based optical fiber sensors: From refractometers to biosensors, *Biosensors* **2017**, *7*, 23.

[37] B. Li, Q. Xue, J. Li, F. Zhang, M. Zou and Y. Yang, Development of a complex gold-immunochromatography test strip for newcastle disease virus and avian influenza virus, *Anim. Husband. Vet. Med.* **2009**, *41*, 33. (In Chinese)